6ICEGE 6th International Conference on Earthquake Geotechnical Engineering
1-4 November 2015
Christchurch. New Zealand

Comparison of Liquefaction-induced Land Damage and Geomorphic Variability in Avonside, New Zealand

S.H. Bastin[1], M.C. Quigley[2], K. Bassett[3]

Abstract

Field mapping, LiDAR, and aerial photography are used to map surface liquefaction-induced lateral spreading fissures and aligned sand blow vents formed during the 22 February 2011 M_w 6.2 Christchurch earthquake. Classification of the study area into 164 polygons enables comparison of liquefaction severity metrics including linear liquefaction feature density, ejecta surface area, and horizontal and vertical ground surface displacements with geomorphic metrics including distance from the downslope free-face, surface elevation, sediment type, and the liquefaction potential index (LPI). Preliminary analyses indicate (i) mean fissure density decreases with increasing distance from the free face at distances of 0-50 m, no relationship is observed at distances >50 m, (ii) mean horizontal ground displacement increases with increasing LPI, and (iii) vertical subsidence is invariant with elevation, implying that other factors (e.g. LPI) may contribute to a complex liquefaction strain field. The basic geology and geomorphology are derived from LiDAR and modern river morphology. Comparison of the liquefaction data with geomorphic mapping indicates geomorphic mapping may be applied to determine the likely distribution of sediments susceptible to liquefaction.

Introduction

Cyclic shearing of loosely consolidated, fluid saturated sediments during earthquake-induced ground motion results in excess pore-water pressures and reduced shear strength in the affected media. Liquefaction occurs as the grain arrangement collapses causing pore water pressures to exceed the confining pressure (Seed & Idriss, 1982; Idriss & Boulanger, 2008). Liquefaction during large earthquakes has resulted in severe damage to land and infrastructure e.g. 1906 San Francisco, 1964 Japan (Idriss & Boulanger, 2008), 1989 Loma Prieta, California (Sims & Garvin, 1995), 1990 Luzon, Philippines (Orense, 2011), 1999 Kocaeli, Turkey (Sonmez et al., 2008), 2010 Haiti (Madabhushi et al., 2013), and the 2010 – 2011 Canterbury Earthquakes (Cubrinovski & Green, 2010; Quigley, et al., 2013). The sedimentological conditions considered highly susceptible to liquefaction are present and former river channels, estuaries, and reclaimed land that is underlain by saturated and loosely consolidated fine sand to silt within 10 m of the surface (Youd & Hoose, 1977; Seed & Idriss, 1982; Idriss & Boulanger, 2008; Orense, 2011; Wotherspoon et al., 2012).

The 2010-2011 Canterbury Earthquake Sequence (CES) caused ≥10 distinct episodes of liquefaction in highly susceptible sediments in parts of eastern Christchurch, New Zealand (Cubrinovski & Green, 2010; Quigley et al., 2013). Liquefaction and liquefaction-induced lateral spreading was primarily concentrated around modern waterways and areas underlain by

[1]Sarah Bastin, Department of Geological Sciences, University of Canterbury, Christchurch, New Zealand, sarah.bastin@pg.canterbury.ac.nz
[2]Dr. Mark Quigley, Department of Geological Sciences, University of Canterbury, Christchurch, New Zealand, mark.quigley@canterbury.ac.nz
[3]Dr. Kari Bassett, Department of Geological Sciences, University of Canterbury, Christchurch, New Zealand, kari.bassett@canterbury.ac.nz

Holocene-to-Recent fluvial deposits that host shallow water tables (<1-2 m; Orsense et al., 2011; Wotherspoon et al., 2012). In this study we compare the distribution of CES liquefaction and associated ground damage with near-surface sedimentologic, topographic, and geomorphic variability in the study area within the suburb of Avonside, eastern Christchurch, to seek relationships between the near-surface properties and observed ground damage.

Geologic Setting

Christchurch is primarily built upon fluvial sand and silt, drained peat swamps, and estuarine, dune, and foreshore sands deposited during sea level regression following a mid-Holocene high-stand that reached up to 3 km inland of the central city at 6.5 ka (Brown & Weeber, 1992). The youthful and unconsolidated nature of these predominately fine sands and silts, combined with shallow water tables (1-2 m depth) and localized artesian water pressures pose a high liquefaction hazard for much of the city (Elder et al., 1991). The study area of Avonside, eastern Christchurch is located in an inner meander bend of the Avon River (Fig. 1). The suburb is underlain by late Holocene fluvial fine sand to silt, and aeolian dune sand (Fig. 1B; Brown & Weeber, 1992).

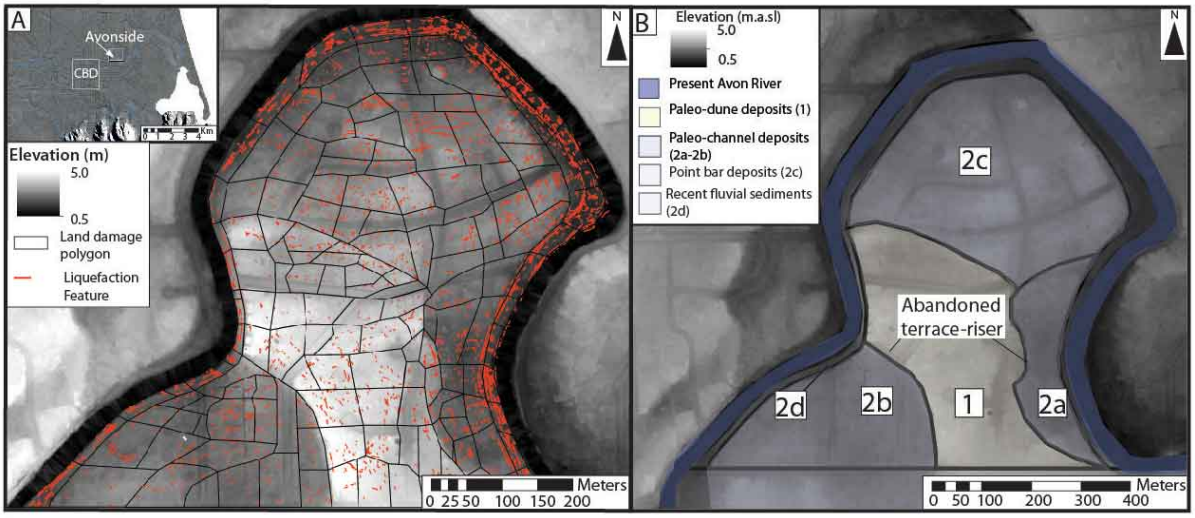

Figure 1: A) 0.5 m LiDAR of Avonside overlain with the 164 land damage polygons and mapped axes of liquefaction features; INSERT: location of Avonside relative to Christchurch CBD B) Basic geologic map of Avonside underlain by the 0.5 m LiDAR.

Methods

The study area was divided into a suite of 164 polygons to document variations in the liquefaction severity following the 22 February 2011 M_w 6.2 earthquake, and the total CES liquefaction-induced ground displacement (Fig 1). Polygons were delineated from variations in elevation, observed liquefaction ejecta, and orientations of the modern Avon River. Elevation data was derived from the 0.5 m LiDAR generated from the LINZ 1:50,000 scale Topographic data layers (https://lris.scinfo.org.nz/layer /187-christchurch-15m-dem-height-corrected). The axes and aerial extent of liquefaction ejecta of 4872 surface liquefaction features comprising linear arrays of sand blows and lateral spreading fissures were mapped in detail using ArcGIS

and the aerial photography flown on 24 February 2011 by NZ Aerial Mapping (NZAM) for the Christchurch Response Centre (imagery available at http://koordinates.com/#/layer/3185-christchurch-post-earthquake-aerial-photos-24-feb2011). The aerial extent of an additional 379 surface flooding features were also mapped. The result was ground-truthed with field mapping in September 2012. Surface liquefaction features mapped on roads and driveways were omitted from further analysis as their orientation and distribution appeared to be controlled by engineered structures. Each polygon was assigned numerical values of linear liquefaction feature and ejecta densities and average CES horizontal and vertical ground displacements (Fig. 2). The linear liquefaction feature and ejecta densities were determined from the number of liquefaction features, and the aerial extent of ejecta divided by the total visible area in each polygon (e.g. not obscured by infrastructure or vegetation). Mapping did not take into account the width of surface features nor the thickness of the ejecta or associated surface flooding. The horizontal and vertical permanent ground displacements were derived by Tonkin and Taylor from comparisons of the changes in location of residential dwellings and infrastructure between the 2008 and September 2011 LiDAR. The result was corrected for the tectonic component using predicted fault displacement from the geodetic models of Beavan et al. (2012).

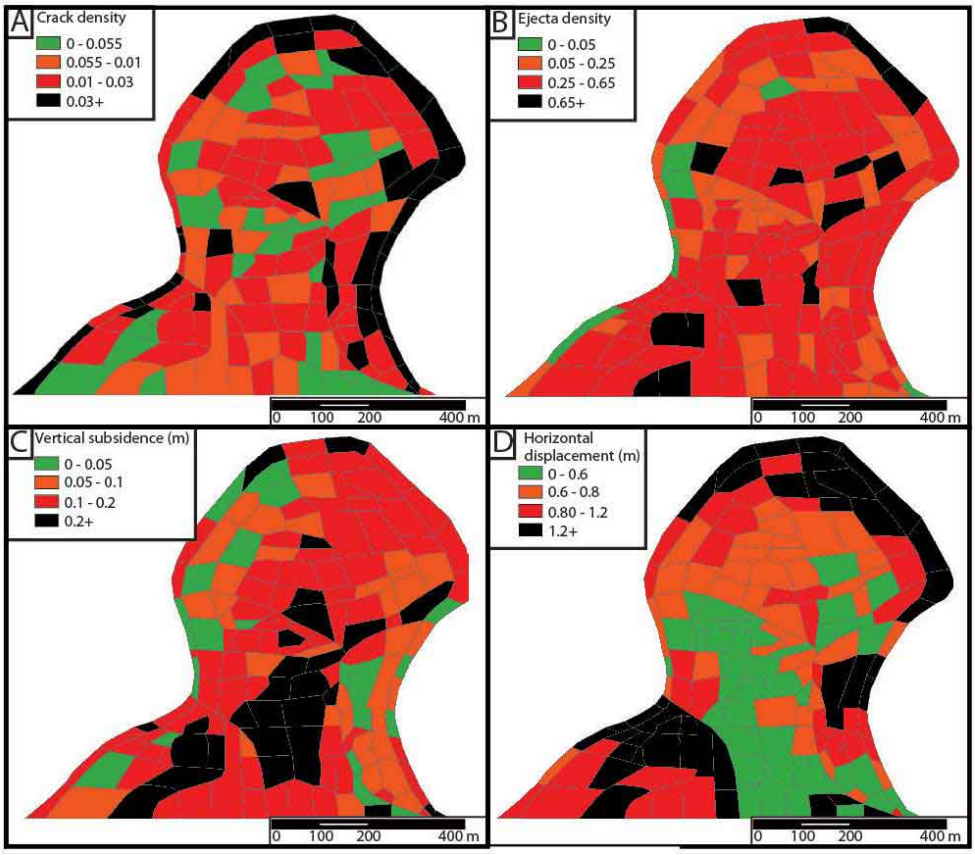

Figure 2: The liquefaction feature (A) and ejecta (B) densities for the 164 land damage polygons and the average CES-induced vertical (C) and horizontal ground displacements (D).

Variations in the Distribution and Severity of Liquefaction

The severity of CES liquefaction-induced ground damage varies across Avonside (Fig. 2). The elevation, sediment type, and distance from the closest down-slope free-face were derived for each polygon to seek relationships between the observed land damage and the near-surface properties (Fig. 3). Here we refer to a 'free-face' as a break in slope such as a river bank or abandoned terrace riser (Fig 1B) that facilitates the down-slope transport of liquefied sediment via basal glide and stretching within the liquefied layer. The subsurface sediment type is inferred from the soil behaviour type index (I_c) and corroborated with sediment descriptions from paleo-seismic trenching work conducted by Bastin et al. (2015; Fig. 3). The I_c was computed from the CPTu soundings conducted in Avonside during the CES using the methodology outlined in Robertson and Wride (1998). The liquefaction-induced damage is also compared to the liquefaction potential index (LPI; Fig. 3D) which predicts the severity of the surficial manifestation of liquefaction based on the thickness, susceptibility, and depth of the potentially liquefied layer(s). The methodology for calculating LPI in post-liquefied soils in the Christchurch region is outlined in Maurer et al. (2014).

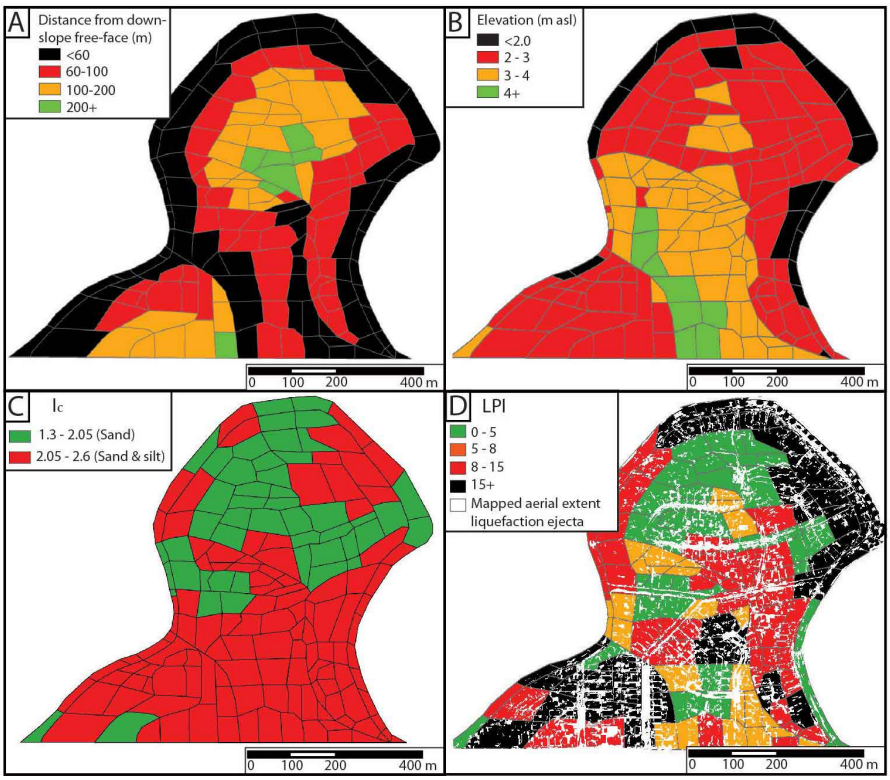

Figure 3: A) Distance of each polygon to the closest downslope free-face. B) Average elevation of each polygon. C) The average I_c for each polygon as derived from post-CES CPTu. D) The average LPI of each polygon overlain with the mapped aerial extent of liquefaction ejecta.

The linear liquefaction features formed in highest abundance adjacent to the free-faces (Fig. 2A). The mean density of linear liquefaction features decreases within 0 to 50 m of the free-faces (as defined by a linear fit with a high R^2; Fig. 4A) at which point the mean liquefaction feature density shows no relationship with increasing distance (Fig. 4A). The standard deviation indicates that the density of linear liquefaction features derived for each polygon is highly

variable within 50 m of the free-faces, this variability decreases with increasing distance possibly due to the decreasing sample sizes. The mean linear liquefaction feature density combined with horizontal displacement also decreases within 50 m of the free-faces beyond which point it shows no relationship with increasing distance (Fig. 4B). The standard deviation indicates that the combined horizontal displacement and linear liquefaction feature density derived for each polygon is highly variable adjacent to the free-faces (0 m). This variability sharply decreases away from the free-faces. The values of linear liquefaction feature density and combined linear liquefaction feature density and horizontal displacement derived for each polygon, and the mean values for each 10 m increment in distance from the free-face are plotted in Fig. 4A and B respectively. Two trend-lines are derived from the mean values to account for the relationships observed in the data (Fig. 4A & B). No relationship is observed between elevation and mean subsidence (Fig. 4C). This trend-line is derived from mean subsidence for each 0.2 m increase in elevation (Fig. 4C). The standard deviation of the subsidence derived for each polygon indicates that subsidence is variable over all elevations (Fig. 4C).

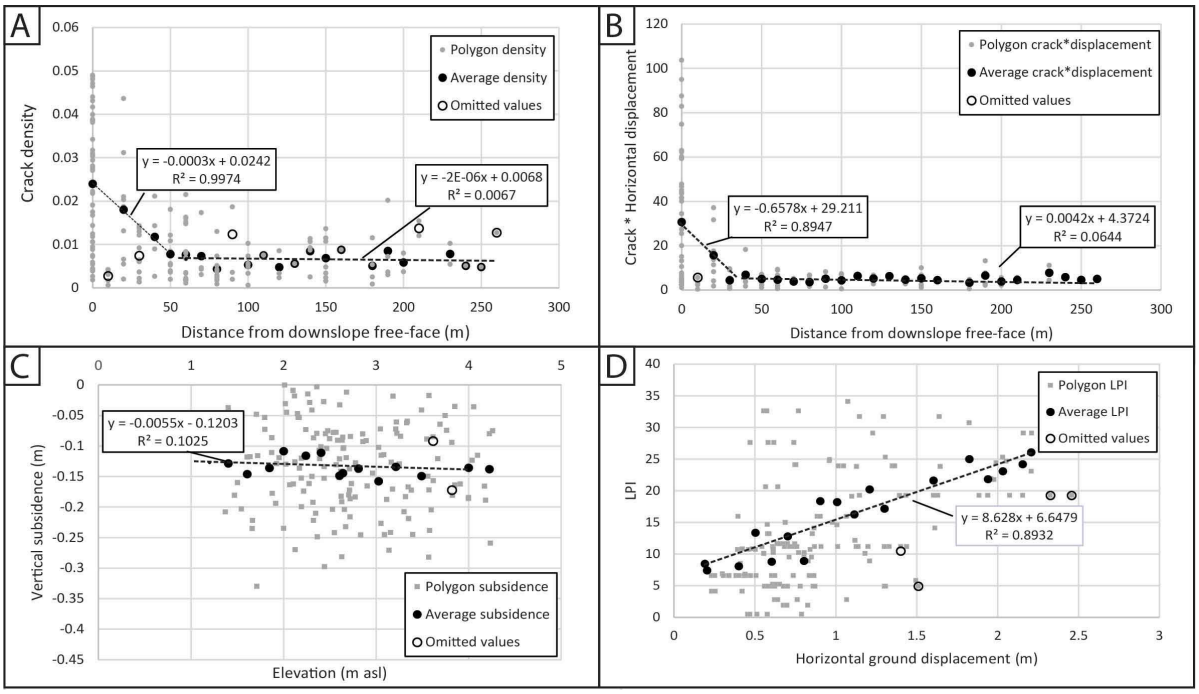

Figure 4: The mean linear liquefaction feature density (A) and combined mean linear liquefaction feature density (LF density) and horizontal displacement (B) decrease within 50 m of the free-face. C) No correlation is observed between mean subsidence and elevation. D) Mean horizontal displacements increases with increasing LPI. INSERTS: Standard deviation of values derived for each polygon compared with increasing distance from the free-face (A & B), elevation (C), and horizontal displacement (D).

The mean horizontal displacement increases with increasing LPI (portrayed by a linear fit in Fig. 4D); polygons exhibiting high LPI values (Fig. 3D) also exhibit high lateral displacements (1.2m+; Fig. 4D). The standard deviation indicates that the LPI of each polygon is highly variable with increasing horizontal displacement. The trend-line is derived for the mean LPI at 0.2 m increments in horizontal displacement (Fig. 4D). Polygons exhibiting high LPI values

correlate with polygons exhibiting high densities of liquefaction ejecta (Fig. 3D). However, the surface manifestation predicted by the LPI under-estimates the observed liquefaction severity (Fig. 3D). This may be attributed to lateral spreading which is not accurately accounted for in the LPI calculation (Maurer et al., 2014).

Relationships between Liquefaction-induced Land Damage and Near-surface Properties

Maximum CES lateral spreading-induced horizontal displacements were recorded adjacent to the river in Avonside. Horizontal displacements decreased with increasing distance from the river with negligible horizontal displacements recorded at 100-150 m (Robinson et al., 2012). The high horizontal displacements recorded proximal to the river correlates with the high densities of linear liquefaction features (Fig. 4A), and combined linear liquefaction feature density and horizontal displacements recorded within 50 m of the free-face (Fig. 4B). This indicates that severe liquefaction-induced damage occurred within 50 m of the free-face during the CES. Comparison of the azimuths of the linear liquefaction features and the closest down-slope free-faces (Fig. 1A) indicates that >70% of the liquefaction features are oriented within 20^{o} of the free-faces and therefore primarily formed sub-parallel to the closest free-face. The decreasing linear liquefaction feature density and combined liquefaction density and horizontal displacement (Fig. 4A & B) within 50 m of the free-faces (Fig. 2A & D) likely results from the decreasing lateral spreading induced horizontal displacements with increasing distance from the free-faces. Comparably lower lateral spreading-induced horizontal displacements at distances >50 m from the free-faces during the CES may account for the lack of correlation between the linear liquefaction feature density and combined horizontal displacement and linear liquefaction density at these distances (Fig. 2A, 4A, & 4B).

No relationship is observed between elevation and mean vertical subsidence (Fig. 4C) however, visual comparison suggests that polygons distal to the free-faces exhibit high subsidence (0.1 m+; Fig. 2C & 3A), while polygons proximal to the free-faces exhibit varied subsidence (0-0.2 m; Fig. 2C). The high subsidence observed distal to the free-faces (Fig. 3B) likely results from lateral spreading causing the down-slope transport of liquefied sediment towards the closest free-face, the ejection of liquefied sediment, and possible densification within the liquefied unit. Subsidence of 0.1 - 0.2 m recorded proximal to the free-faces may result from the transport of liquefied sediment into the modern river channel. Comparably lower subsidence of 0-0.1 m recorded proximal to the free-faces may reflect deformation associated with the cessation of lateral-spreading adjacent to the free-faces and uplift within the modern river (Fig. 2C; Hughes et al., 2014). Polygons exhibiting elevations >3 m generally exhibit high subsidence (0.2 m+) and low LPI (Figs. 2C, 3B & D). This likely results from the comparatively lower-water table in these polygons. The water-table is tidally influenced and controlled by the height of the Avon River which remains approximately at sea level. High vertical subsidence is also observed in polygons with elevations < 2 m and high LPI (Fig. 2C, 3B & D). This indicates that elevation exerts a weak control on the severity of vertical subsidence which may be overwritten by higher LPIs.

Other factors that may have influenced the variability in the severity of liquefaction include, but are not limited to, the slope across the polygon and the depth to the first liquefiable layer. This data was not incorporated into the current analysis as the data as it was not readily available, however it will be incorporated into future analyses.

Comparison with the Geomorphology of Avonside

The geomorphology of the study area is mapped from the 0.5 m LiDAR data combined with the present morphology of the Avon River (Fig. 1B). Zone 1 comprises the central, higher elevation area that contains Holocene sand dune deposits and overbank fluvial deposits, as indicated in the Christchurch geological map (Brown & Weeber, 1992). Zone 2 comprises the surrounding lower elevation areas of Late Holocene fluvial deposits of the Avon River (Fig. 1B). The sharp elevation contrasts along the eastern and western margins of Zone 1 are interpreted as abandoned terrace risers (Fig. 1B). The abandoned terrace risers and morphology of Zones 2a and 2b indicate that these areas were formerly occupied by the Avon River and thus comprise paleo-channels. Zone 2b is interpreted to comprise paleo-channel deposits of unconsolidated, saturated sandy silt underlain by fine sand (Bastin et al., 2015). The morphology and higher elevations of Zone 2c suggests that it comprises point bar deposits from the outward migration of the Avon River channel (Fig. 1B). The areas within 50 m of the Avon River (2d) are most likely underlain by recent, unconsolidated and saturated fine sand to silt of over bank deposits from the Avon River.

The unconsolidated and saturated fine sand to silt comprising the paleo-channel and over-bank deposits (Zones 2b, c, and d) are anticipated to be highly susceptible to liquefaction, which is supported by their high LPI (Fig. 3D). These paleo-channels and recent fluvial deposits exhibit high densities of linear liquefaction features and ejecta, and high horizontal displacements further supporting that they are underlain by sediments highly susceptible to liquefaction (Fig. 1B & 3). Zone 1 exhibits comparatively less liquefaction-induced damage than the other zones, possibly due to the comparatively older age of the sediment overlying the liquefiable stratum and/ or the higher elevations (>3 m; Brown & Weeber, 1992; Bastin et al., 2015). Geomorphic mapping combined with the variations in CES liquefaction and ground displacements indicate that the areas within 50 m of the river and underlain by recent fluvial sediments exhibited severe liquefaction-induced damage during the CES (Fig. 1B). The correlations between the liquefaction-induced damage and the geomorphology of Avonside indicates that depositional setting and proximity to the free-faces exert first order influences on the liquefaction potential of the polygon. This also highlights the small scale heterogeneity of sedimentary deposits within fluvial depositional, and the potential limitations of site-specific geotechnical testing in determining subsurface sediment type and the overall liquefaction potential of a given area. Initial paleo-liquefaction investigations in the paleo-channel (Zone 2b) and point-bar (Zone 2c) deposits in Avonside revealed pre-CES liquefaction dated to post 1660 to pre ca. 1905 confirming that the area has previously liquefied (Bastin et al., 2015).

Conclusions

The main factors influencing the distribution and severity of liquefaction within Avonside are distance from a free-face being the modern river banks or abandoned terrace risers, and depositional setting, while elevation exerts a second order influence. Areas within 50 m of a free-face exhibited severe liquefaction-induced damage during the CES. Comparably less severe liquefaction-induced damage was observed in higher elevation (3 m+) areas at distances >50 m from a free-face (e.g. Zone 1). Geomorphic mapping combined with the mapped liquefaction features and horizontal displacements indicates that the sediments most susceptible to liquefaction are recent fluvial and paleo-channel deposits. The LPI linearly increases with

horizontal ground displacement, although the LPI under-estimates the severity of the surface manifestation of liquefaction in the study area possibly due to lateral spreading.

The LiDAR combined with river morphology enables interpretation of the basic geologic and geomorphic variability within the study area. Comparison of the liquefaction data with near-surface properties highlights the potential application of geomorphic mapping to determine the likely distribution of potentially liquefiable sediments within fluvial settings. Understanding how the liquefaction-induced damage varies within these fluvial settings (i.e. between paleo-channels and point bars) may be used to target sites for geotechnical testing.

Acknowledgments

We thank Dr. Sjoerd van Ballegooy of Tonkin & Taylor for providing data and discussions which aided the data interpretation of the mapped data. We also thank Matthew Hughes for his assistance with ArcGIS. This work was funded by an EQC Capability Fund.

References

Bastin SH, Quigley MC, Bassett K. Paleo-liquefaction in Christchurch, New Zealand. *Geological Society of America Bulletin*, 2015; doi: 10.1130/B31174.1.

Beavan J, Levick S, Lee J, Jones K. *Ground displacements and dilational strains caused by the 2010-2011 Canterbury earthquakes.* GNS Science Consultancy Report 67, Lower Hutt, New Zealand, 2012.

Brown LJ, & Weeber JH. *Geology of the Christchurch Urban Area*. Scale 1:25 000. Institute of Geological and Nuclear Sciences geological map 1. 1 sheet + 105 p: Institute of Geological and Nuclear Sciences Limited, Lower Hutt, New Zealand, 1992.

Cubrinovski M, & Green RA (eds.). Geotechnical Reconnaissance of the 2010 Darfield (Canterbury) Earthquake, (contributing authors in alphabetical order: J. Allen, S. Ashford, E. Bowman, B. Bradley, B. Cox, M. Cubrinovski, R. Green, T. Hutchinson, E. Kavazanjian, R. Orense, M. Pender, M. Quigley, and L. Wotherspoon). Bulletin of the *New Zealand Society for Earthquake Engineering* 2010; **43** (4): 243-320.

Elder DM, McCahon IF, Yetton MD. *The earthquake hazard in Christchurch: a detailed evaluation*. Research report to the EQC, Soils and Foundations Ltd., Christchurch, New Zealand, 1991.

Hughes MH, Quigley MC, van Ballegooy S, Deam BL, Bradley BA, Hart DE. The sinking city: Earthquakes increase flood hazard in Christchurch, New Zealand. *GSA Today* 2014; **25** (3–4): 4-10.

Idriss, IM, & Boulanger RW. *Soil Liquefaction during Earthquakes*, Monograph Series: Earthquake Engineering Research Institute, Oakland, California, 2008.

Maurer BW, Green RA, Cubrinovski M, Bradley B. Evaluation of the Liquefaction Potential Index for Assessing Liquefaction Hazard in Christchurch, New Zealand. *Journal of Geotechnical and Geoenvironmental Engineering* 2014; **140** (7): 04014032-1-11

Madabhushi SPG, Saito K, Booth ED. EEFIT mission to Haiti following the 12th January 2010 earthquake. *Bulletin Earthquake Engineering* 2013; **11**: 35–68.

Orense RP. Soil liquefaction during the 2010 Darfield and 1990 Luzon Earthquakes: A comparative study: Proceedings of the *Ninth Pacific Conference on Earthquake Engineering Building an Earthquake-Resilient Society* 14-16 April, Auckland, New Zealand, 2011.

Quigley MC, Bastin S, Bradley BA. Recurrent liquefaction in Christchurch, New Zealand, during the Canterbury earthquake sequence. *Geology* 2013; **41** (4): 419-422.

Reid, CM, Thompson NK, Irvine JRM, Laird TE. Sand volcanoes in the Avon-Heathcote estuary produced by the 2010-2011 Christchurch earthquakes: Implications for geological preservation and expression. *New Zealand Journal of Geology and Geophysics* 2012; **55** (3): 249-254.

Robertson, P.K. & Wride, C.E. Evalulating cyclic liquefaction potential using the cone penetration test. *Canadian Geotechnical Journal*, 1998, **35**(3): 442-459.

Robinson, K., Bradley, B.A., Cubrinovski, M. Analysis of Liquefaction-induced lateral spreading data from the 2010 Darfield and 2011 Christchurch earthquakes, *Proc. New Zealand Society for Earthquake Engineering Conference*, Christchurch, New Zealand 2012.

Seed HB & Idriss IM. *Ground Motions and Soil Liquefaction during Earthquakes*, Monograph Series: Earthquake Engineering Research Institute, Berkeley, California, 1982.

Sims JD, Garvin CD. Recurrent Liquefaction Induced by the 1989 Lorna Prieta Earthquake and 1990 and 1991 Aftershocks: Implications for Paleoseismicity Studies. *Bulletin of the Seismological Society of America* 1995; **85** (I): 51-65.

Sonmez B, Ulusay R, Sonmez H. A study on the identification of liquefaction-induced failures on ground surface based on the data from the 1999 Kocaeli and Chi-Chi earthquakes. *Engineering Geology* 2008; **97** 112–125.

Wotherspoon LM, Pender MJ, Orense RP. Relationship between observed at Kaiapoi following the 2010 Darfield earthquake and former channels of the Waimakariri River: *Engineering Geology* 2011; **125**(2): 45 – 55.

Youd TL, & Hoose S. Liquefaction Susceptibility and Geological Setting, *Proc., 6th World Conf. on Earthquake Engineering*, Vol. 3, Prentice-Hall, Englewood Cliffs, N.J., 1977.